IEEE Access
Multidisciplinary | Rapid Review | Open Access Journal

Received November 2, 2017, accepted January 13, 2018, date of publication February 8, 2018, date of current version March 12, 2018.

Digital Object Identifier 10.1109/ACCESS.2018.2796625

In Vivo Fascicle Bifurcation Imaging of Rat Sciatic Nerve Using Swept-Source Optical Coherence Tomography

DAEYOUNG CHOI, JAEYUL LEE, MANSIK JEON, AND JEEHYUN KIM

School of Electronics Engineering, College of IT Engineering, Kyungpook National University, Daegu 41566, South Korea

Corresponding author: Mansik Jeon (msjeon@knu.ac.kr)

This work was supported in part by the Ministry of Education through BK21 Plus project, South Korea, under Grant 21A20131600011 and in part by the Bio and Medical Technology Development Program of the NRF through the Korean Government, MSIP, under Grant 2017M3A9E2065282.

ABSTRACT The sciatic nerve is the longest and widest single nerve in the human body and is responsible for the signal transduction of the entire hind limb region. Its wide nerve dynamic range and size makes it sensitive to injury. The branching and location of the sciatic nerve are important, and unlike histology, optical coherence tomography (OCT) can provide rapid non-destructive cross-sectional images. The sciatic nerves of ten rats were analyzed using swept-source (SS)-OCT. The sufficient depth penetration of the SS-OCT system allowed clear identification of the internal bifurcation point of the external branching and the internal route for the three terminal nerves in cross-sectional images. Internal bifurcation is observed through interfascicular epineurium resulting from epineurium division. Two bifurcations occur at the bottom of the sciatic nerve. The first and second bifurcations occur approximately 7 and 5 mm, respectively, above the external branching. SS-OCT enabled visualization of surgical needle positioning during direct injections into the sciatic nerve, which is beneficial for drug injection or microelectrode placement for electrical signal processing as a nerve detection guide. Therefore, analysis of the internal structure obtained in real time and needle position information inside the nerve are expected to act as a guide for neurosurgery.

INDEX TERMS Nerves, sciatic nerve, intraneural injection, bifurcation, swept-source optical coherence tomography.

I. INTRODUCTION

The sciatic nerve is a large, long single nerve (the longest and thickest single nerve in the human body) responsible for movements in the entire hind limb of animals. The sciatic nerve arises from L4 (lumbar vertebrae position) to S3 (sacral vertebrae position), a collection of nerve fibers that emerge from the sacral part of the spinal cord in the human-body [1], [2]. Signal transduction of the sciatic nerve involves muscle movements and skin awareness in the hind limb region. Therefore, when problems occur in the sciatic nerve, hind limb movements and skin awareness may be affected. Several pathological problems can occur due to damage of the sciatic nerve, such as sciatica, injury through deep intramuscular injections, piriformis syndrome, and sciatic nerve block failure. [3], [4]. Treatment and pain relief of these diseases requires an internal and external handle for the sciatic nerve. Especially, the failure of deep intramuscular injection, intraneural injection and sciatic nerve block are iatrogenic problems. The branching and location of the sciatic that occurs when localization of the sciatic nerve fails, is the major cause of sciatic nerve damage according to major medicolegal claims [5]–[7]. Intraneural needle trauma or injection are major risk factors, which can be occured while perfoming the surgeries for the aforementioned diseases. Minimizing the error for the localized placement of the needle or local anesthetic solution can eliminate the major risk factors for the nerve. Conventional techniques have advantages in extraneural placement, however, techniques for handling intraneural placement in real-time are scarce.

Nerves diseases may be caused by internal or external damage. Because of the characteristics of the nerve derived from the root, the point of injury and the point of pain may be different. Since the internal structure is deformed according to the bifurcation point, it is necessary to obtain the exact positions of the internal and external bifurcations.

Hence, quantitative analysis of the sciatic nerve or branching is needed for precise treatment and pain relief in related diseases. The sciatic nerve is divided into three peripheral nerves in the rat: the fibular, tibial, and sural nerves. These three nerves are divided into three different positions depending on the nerve signal transduction [8], [9]. Several bundles proceeding from L4 and L5 (sometimes L6) are merged into a single bundle. However, when L4 and L5 (sometimes L6) are independent, each nerve fiber has its own epineurium. Thus, a precise understanding regarding the formation of nerve fibers is essential, and internal bifurcation is not limited to structural branching alone, but it can also provide a structural framework of neuronal interactions.

To gain a better understanding of the branching of the sciatic nerve, histological experiments have been performed to observe the microanatomy of its tissues. Nevertheless, nerves can be damaged during histological observation of the sciatic nerve [10]. Moreover, techniques such as computed tomography (CT), ultrasound (US), and magnetic resonance imaging (MRI) are unable to acquire images of the internal structure of the sciatic nerve due to their low resolution [11], [12]. Sciatic nerves can also be damaged or ionized while using these techniques.

Optical coherence tomography (OCT) is an ideal method to detect nerve structures due to its non-invasive, non-ionizing, and high-resolution properties [13]–[17]. In addition, rapid real-time imaging technique can be used to identify the structures of living organisms, for functional observation of organisms, and for pharmacokinetics. Due to the micrometer resolution and three-dimensional (3D) imaging capability, OCT can detect nerves internally and externally with sufficient resolution. Therefore, it enables observation of the bifurcation of fascicles in the sciatic nerve and provides a better understanding of how the internal sciatic nerve fascicles are constructed and divided. Previously, neurological OCT studies were performed on micro units, but our study is focused on structural changes due to bifurcation. Thus, our OCT with high-resolution and high-penetration features can reflect all the information about the inside of the sciatic nerve that is important in medical surgery [18], [19].

In this study, an external structure for the sciatic nerve was formed and further internal bifurcation was detected. By distinguishing between the inner and outer membrane boundaries of the nerve's external bifurcation and nerve bundle, OCT can be used as a guide for electrical signal processing and drug injection inside the fascicle [20]–[22].

II. MATERIALS AND METHODS

A. SAMPLES PREPARATION OF IN VIVO ANIMAL MODELS

The animal experiments were conducted in accordance with the guidelines of the Institutional Animal Care and Use Committee of Kyungpook National University. Ten sciatic nerve specimens (Sprague Dawley rats 5 to 8 weeks old weighing 130-170 mg) were used. Each rat was placed in an anesthetic cage for 5 minutes, and anesthesia was induced with oxygen mixed with 1% isoflurane. Once the anesthesia was successfully completed, the rat was placed on the operating table and a mouthpiece was mounted to administer anesthetic gas to maintain continuous anesthesia during the surgical procedure. To obtain the in vivo sciatic nerve images, the hair of both hind limbs were removed. The skin and muscles covering the nerve were surgically removed. To obtain a clean image free of impurities, the sciatic nerve was washed with phosphate-buffered saline (PBS) and pH 7.4, to minimize biological reactions. During the imaging, PBS was continuously sprayed on the nerve to prevent dehydration. The experiment was carried out at room temperature (24 °C). After obtaining the images, the rats were euthanized and disposed of at the designated location according to the guidelines for animal processing.

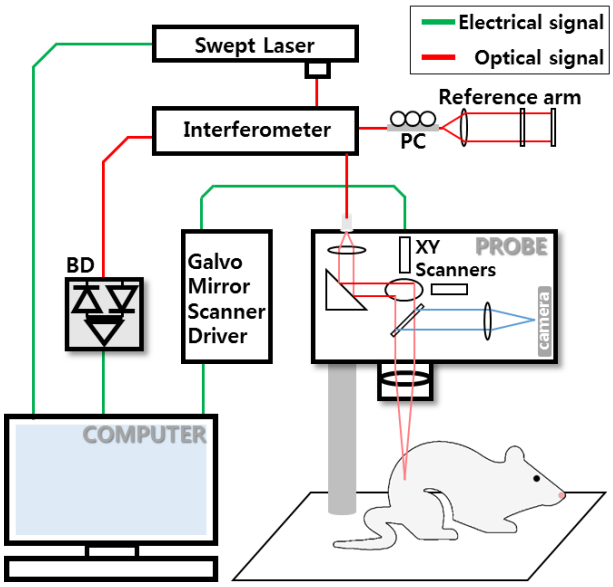

FIGURE 1. Schematic of 1300-nm SS-OCT system. BD: balanced detector; PC: polarization controller; swept laser: MEMS VCSEL swept laser.

B. OCT SYSTEM CONFIGURATION

The swept-source (SS)-OCT system (OCS1310V1 OCT Thorlabs Inc.) used has a center wavelength of 1300 nm and a spectral bandwidth of >97 nm. The coherence length is 50 mm and the axial scan rate is 100 kHz. Therefore, it is possible to acquire 200 B-scans per second with 500 axial scans within 2.5 seconds to construct a single 3D image. The resolution of the 2D cross sectional image is 25 μm in transverse and 16 μm in axial direction, respectively. The maximum volume size is 10 mm × 10 mm × 12 mm. A schematic of the OCT system is shown in Figure 1. The sample was placed underneath the probe and the X, Y stage was used for specimen rotation. A charge-coupled device (CCD) provided a microscopic view of the sample. CCD images and OCT images were acquired in real time. The acquired real-time two-dimensional (2D) images were post processed for

the reconstruction of 3D images using volumetric imaging software.

The 2D images with a size of 309 × 509 pixels were obtained from in vivo samples. The field of view of the sciatic nerve specimens was 3 mm × 10 mm. After real-time image acquisition, we used 500 b-scan cross-sectional images obtained in real-time to obtain post-processed rendering images. The quantitative assessment was performed using a customized automated program coded using MATLAB® to obtain amplitude scans (lateral direction intensity fluctuation) in transverse directions for evaluating the microstructures in the lateral direction.

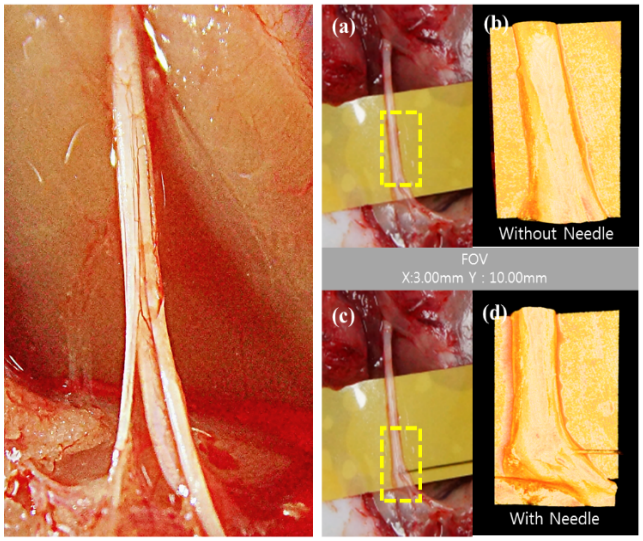

FIGURE 2. Left side: external image of the sciatic nerve. Right side: (a) Sciatic nerve; (b) Rendered image without needle. (c) Sciatic nerve with needle (d) Rendered image with needle. Yellow outlined box is the field of view of the rendered images.

III. RESULTS

A. INTERNAL AND EXTERNAL IMAGES OF THE SCIATIC NERVE

We were able to obtain images with a CCD camera by first surgically exposing the sciatic nerve within the muscle. The large image shown in Figure 2 depicts the external appearance of the sciatic nerve, which consists of one bundle that then divides into three distal nerves. The sciatic nerve is merged with L4 and L5 (sometimes L6) nerves, and the merged nerves cannot be identified visually as shown in Figure 2. The sciatic nerve is then divided into the fibular nerve, tibial nerve, and sural nerve. Each nerve transmits nerve impulses to its own region of the body. However, whether the nerve fibers in the sciatic nerve are fused to each other or whether L4 and L5 (L6) fascicles remain separate from the vertebrae and separate from each other has not been able to be observed. Thus, the formation (or not) of a bifurcation would distinguish between these two possibilities.

Figure 2 shows the CCD and 3D OCT views of the sciatic nerve with and without needle penetration with a field of view of 3 × 10 mm. As shown in the image, the sciatic nerve was placed on a thin film layer to separate it from muscles and other tissues in order to observe only the sciatic nerve bundle. Later, the sciatic nerve was washed with PBS to remove impurities.

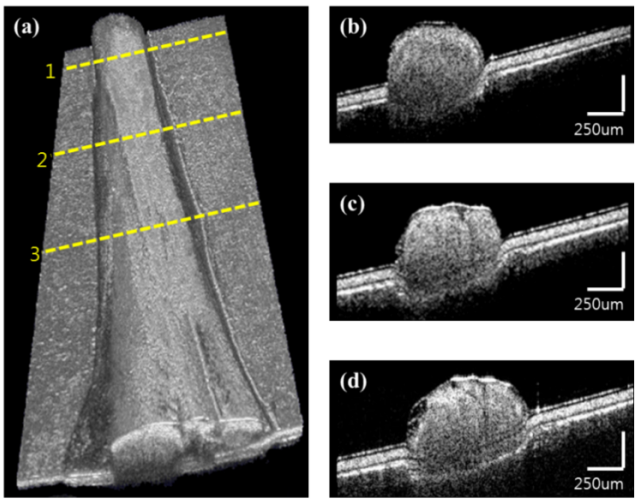

FIGURE 3. OCT images of sciatic nerve on a support fixture. (a) Three-dimensional rendered image of the sciatic nerve. (b)–(d) B-scan images corresponding to yellow dashed lines 1–3 in (a). (d) Tibial nerve, fibular nerve, and sural nerve from left to right. The support fixture is vinyl tape. The field of view in (a) is 3.00 mm (X) × 10.00 mm (Y) × 2.0 mm (Z).

The 3D OCT image of the sciatic nerve after volume rendering is shown in Figure 3(a) and the correlated cross-sectional images are shown in Figure 3(b)–(d). In Figure 3(b), a single fascicle can be observed without a compartment. This confirms that the nerve fibers inside the L4 and L5 (L6 in each) descending from the spinal cord are wrapped in one perineurium and fused into one fascicle. Figure 3(c) provides a clear visualization of the bifurcation in the middle of the sciatic nerve. Fascicles are divided into perineurium and interfascicular epineurium due to the clearly visible bifurcation. Between the fascicles is the interfascicular epineurium. Quantitatively, image analysis revealed the position of the first bifurcation at approximately 7 mm above the external branching position. This was based on the point where the branching can be visually identified. Figure 3(d) depicts more compartments, and thus an additional interfascicular epineurium can be seen. This point is 5 mm above the branching point. Eventually, three bundles of fascicles emerge. The external bifurcation of the sciatic nerve is formed at the bottom of Figure 3(a). However, the initial two consecutive bifurcations later develop and branch into three bifurcations. In Figure 3(d), three differentiated nerves can be detected, from left to right: the tibial, fibular, and sural nerves. Finally, they are not differentiated from their respective independent lumbar nerves. It can be seen that the fibers are fused with one fascicle and then divided into three.

B. EN FACE IMAGE OF SCIATIC NERVE BIFURCATION

To apply OCT as a surgical tool for the sciatic nerve, we need a complete coordinate system of 3D bifurcation points. By acquiring en face images of the sciatic nerve,

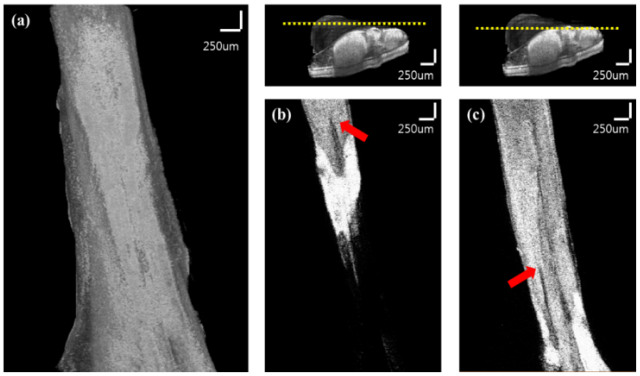

FIGURE 4. En face image of the sciatic nerve. (a) Upper region of the sciatic nerve. (b) and (c) En face images corresponding to the yellow dashed lines above.

detailed information can be obtained about the bifurcation point about the Z-axis. Figure 4(a) shows the upper region of the sciatic nerve but provides no information regarding the bifurcation point externally. Figure 4(b) and (c) are the en face images rendered from 3D images. In Figure 4(b), the image is shifted approximately 100 μm from the top of the sciatic nerve to the bottom of the Z-axis. Depending on the position, the thickness of the sciatic nerve is different and the lower part is not visible. However, the region indicated by the red arrow in Figure 4(b) shows complete separation of the fascicle into two parts, confirming that the interfascicular epineurium is a bifurcation point. The sciatic nerve consists of two perineuriums in one nerve bundle. The second bifurcation point can be detected below 200 μm. The interfascicular epineurium made at the second bifurcation point was confirmed in the en face image in Figure 4(c). However, owing to the complexity of the 3D structure of the bifurcation, it is obscured by the structure and appears to be invisible owing to the shallow penetration depth. However, the interfascicular epineurium was exposed near the surface of the sciatic nerve, confirming the junction of the three lines using OCT. It was confirmed that this was connected to the last three ends of the sciatic nerve.

C. EVALUATION OF RAT SCIATIC NERVE BIFURCATION THROUGH LATERAL DIRECTION INTENSITY FLUCTUATION PROFILES

This quantitative evaluation was performed to confirm the bifurcation point of the sciatic nerve with objective evidence. The lateral direction intensity fluctuation profile was performed at the point where the interfascicular epineurium inside the sciatic nerve was located as evidence of bifurcation. The fascicle is a highly scattering medium with a higher intensity than the interfascicular epineurium.

The interfascicular epineurium confirms the bifurcation, showing 70% lower intensity than the inside of the fascicle. The interfascicular epineurium was considered as objective evidence for bifurcation as a gap due to the distribution of the fascicles. The intensity analysis program was coded using MATLAB®. Each image was loaded first for analysis. The red lines shown in Figure 5 illustrates lateral direction three intensity lines, which were later summed up and averaged to obtain the pixel intensity plot. The intensity representation shown in the graphs provide a relative representation of the quantitative value of the scatter signal obtained from the sample. By comparing these values, the degree of contrast can be compared. In Figure 5(a), no interfascicular epineurium is seen. Likewise, analysis of the lateral direction intensity fluctuation profile of the interfascicular epineurium space (Figure 5(d)) does not demonstrate a low-intensity fluctuation, which clearly correlates to Figure 5(a). In Figure 5(b), the interfascicular epineurium space accurately matches with the lateral direction intensity fluctuation profile shown in Figure 5(e). Similarly, the image in Figure 5(c) matches the data presented in Figure 5(f). The results obtained from the lateral direction intensity fluctuation profile of Figure 5(c) illustrate a clear correlation with the obtained OCT image and confirms the bifurcation. Therefore, it can be confirmed that OCT can be an ideal non-destructive surgical tool for the detection of microstructure of the sciatic nerve with no large error.

D. SCIATIC NERVE WITH SURGICAL NEEDLE FOR INTRANEURAL INJECTION

Understanding the electric signal transmission according to the sciatic nerve branching is an essential requirement in surgery. Intraneural injection for signal detection or injection requires acquisition of structural information through functional histology. Therefore, as an initial feasibility test, we further extended our experiment by inserting a surgical needle inside the sciatic nerve. We investigated how feasible the implemented SS-OCT system was to detect the needle insertion non-destructively. The difference between the branching points were well visualized from the obtained cross-sectional and 3D OCT images.

Figure 6(a) is a 3D rendered image obtained using volumetric software. The obtained 3D OCT image along with en face and cross-sectional images provide a clear view of needle insertion, and the corresponding fascicle information can be distinguished as well. Figure 6(c) is the cross-sectional image of the point where the needle penetrates. The refractive index values of the air and the sciatic nerve are different, so the needle does not appear linear, but there is no big problem in terms of position. It can be seen that the needle passed through all three fascicles. This provides accurate 2D needle position information. Since the needle pierced diagonally from the right side, the position information of the needle about the Z-axis can be obtained through the en face image. Figure 6(d) is the corresponding en face image obtained from the depth range (yellow dotted line) of Figure 6(b). The ability to use OCT to guide surgical needle positioning suggests that, in vivo observation may allow needle insertion into selected fascicles, thus controlling each internal fascicle of the sciatic nerve. Finally, it can also prevent damage to nerves or other unrelated structures. Thus, future studies can be performed on surgical procedures using the electronic

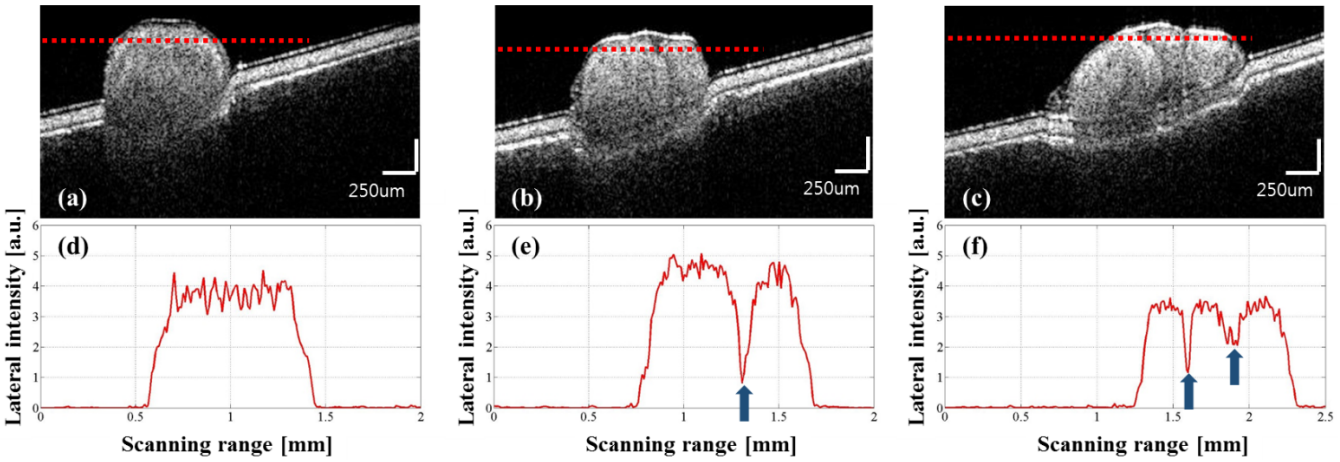

FIGURE 5. Lateral direction intensity fluctuation of sciatic nerve cross-sectional images. (a)-(c) Cross-sectional images of the sciatic nerve. (d)-(f) Analysis of the bifurcation points.

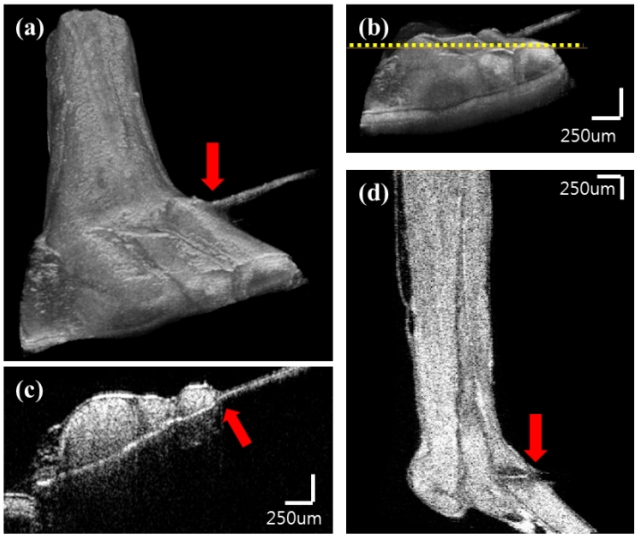

FIGURE 6. Image of the sciatic nerve image with a tungsten needle. (a) 3D rendered images with a needle. (b) A image represented by the baseline of the enface image. (c) Cross-sectional image of the sciatic nerve with needle at a pass point. (d) En face image of the sciatic nerve enface confirming that the needle is inserted.

response of each fascicle directly by inserting a needle with OCT guidance.

IV. CONCLUSION

In this study, the divergence point of the sciatic nerve was non-destructively identified using OCT. Owing to the fast acquisition speed of the 1300-nm SS-OCT system, we were able to acquire rapid cross-sectional images and 3D rendered images of the sciatic nerve in real time. The actual size of the sciatic nerve and the quantitative size of the internal fascicles were obtained through the lateral direction intensity fluctuation profile processing. Two bifurcations occurred in the sciatic nerve from the spine to the feet. Owing to this bifurcation, the sciatic nerve is not composed of individual independent fascicles but merged into a single fascicle. The fascicle then divides again once it reaches toward the end. All the aforementioned structural formations were precisely confirmed through the acquired SS-OCT images. In addition, while inserting a needle to confirm the electrical signal transmission, it was possible to accurately identify the position of the needle despite the strong scattering of the tungsten needle. Although the 3D images were reconstructed by using a post-processing technique, the exact location of the needle was confirmed through real-time cross-sectional images. The obtained results clearly revealed the needle penetration. Subsequently, the obtained results confirmed that OCT can play a major role in needle guidance, which can be used as a non-destructive inspection tool for sciatic nerves, leading to advances in nervous system surgery. Moreover, similar experimental process can be demonstrated for the identification of other nerves, which sufficiently satisfies the resolution parameters of the SS-OCT. Therefore, the animal model experiment in this study provides an informative path and confirms the applicability of the developed inspection protocol for future related experiments.

REFERENCES

[1] B. A. Berihu and Y. G. Debeb, "Anatomical variation in bifurcation and trifurcations of sciatic nerve and its clinical implications: In selected University in Ethiopia," *BMC Res. Notes*, vol. 8, p. 633, Nov. 2015.

[2] J. D. Vloka, A. Hadžić, E. April, and D. M. Thys, "The division of the sciatic nerve in the popliteal fossa: Anatomical implications for popliteal nerve blockade," *Anesthesia Analgesia*, vol. 92, no. 1, pp. 215–217, 2001.

[3] J.-P. Valat, S. Genevay, M. Marty, S. Rozenberg, and B. Koes, "Sciatica," *Best Pract. Res. Clin. Rheumatol.*, vol. 24, no. 2, pp. 241–252, 2010.

[4] L. M. Fishman *et al.*, "Piriformis syndrome: Diagnosis, treatment, and outcome—A 10-year study," *Arch. Phys. Med. Rehabil.*, vol. 83, no. 3, pp. 295–301, 2002.

[5] P. Mishra and M. D. Stringer, "Sciatic nerve injury from intramuscular injection: A persistent and global problem," *Int. J. Clin. Pract.*, vol. 64, no. 11, pp. 1573–1579, 2010.

[6] F. J. Singelyn, F. Aye, and J. Gouverneur, "Continuous popliteal sciatic nerve block: An original technique to provide postoperative analgesia after foot surgery," *Anesthesia Analgesia*, vol. 84, no. 2, pp. 383–386, 1997.

[7] F. Asato, M. Butler, H. Blomberg, and T. Gordh, "Variation in rat sciatic nerve anatomy: Implications for a rat model of neuropathic pain," *J. Peripheral Nervous Syst.*, vol. 5, no. 1, pp. 19–21, 2000.
[8] J. B. Stiehl and W. A. Stewart, "Late sciatic nerve entrapment following pelvic plate reconstruction in total hip arthroplasty," *J. Arthroplasty*, vol. 13, no. 5, pp. 586–588, 1998.
[9] F. Viterbo, A. G. Salvio, B. L. Griva, and F. O. Maciel, "The embracing end-to-side neurorrhaphy in rats," *Acta Cirurgica Brasileira*, vol. 27, no. 3, pp. 260–265, 2012.
[10] H. Schmalbruch, "Fiber composition of the rat sciatic nerve," *Anatomical Rec.*, vol. 215, no. 1, pp. 71–81, 1986.
[11] S. Waag, M. H. Stoffel, C. Spadavecchia, U. Eichenberger, and H. Rohrbach, "Ultrasound-guided block of sciatic and femoral nerves: An anatomical study," *Lab. Animals*, vol. 48, no. 2, pp. 97–104, 2014.
[12] A. M. Lewis, R. Layzer, J. W. Engstrom, N. M. Barbaro, and C. T. Chin, "Magnetic resonance neurography in extraspinal sciatica," *Arch. Neurol.*, vol. 63, no. 10, pp. 1469–1472, 2006.
[13] D. Huang *et al.*, "Optical coherence tomography," *Science*, vol. 254, no. 5035, pp. 1178–1181, 1991.
[14] J. Lee *et al.*, "Decalcification using ethylenediaminetetraacetic acid for clear microstructure imaging of cochlea through optical coherence tomography," *J. Biomed. Opt.*, vol. 21, no. 8, p. 081204, 2016.
[15] M. Jeon, J. Kim, U. Jung, C. Lee, W. Jung, and S. A. Boppart, "Full-range k-domain linearization in spectral-domain optical coherence tomography," *Appl. Opt.*, vol. 50, no. 8, pp. 1158–1163, 2011.
[16] M. F. Shirazi, R. E. Wijesinghe, N. K. Ravichandran, P. Kim, M. Jeon, and J. Kim, "Dual-path handheld system for cornea and retina imaging using optical coherence tomography," *Opt. Rev.*, vol. 24, no. 2, pp. 219–225, 2017.
[17] M. F. Shirazi, R. E. Wijesinghe, N. K. Ravichandran, M. Jeon, and J. Kim, "Dual illumination for cornea and retina imaging using spectral domain optical coherence tomography," *Proc. SPIE*, vol. 10251, pp. 102511G-1–102511G-3, Apr. 2017.
[18] J. Gadsden, K. Gratenstein, and A. Hadzic, "Intraneural injection and peripheral nerve injury," *Int. Anesthesiol. Clin.*, vol. 48, no. 4, pp. 107–115, 2010.
[19] C. A. Chlebicki *et al.*, "Preliminary investigation on use of high-resolution optical coherence tomography to monitor injury and repair in the rat sciatic nerve," *Lasers Surg. Med.*, vol. 42, no. 4, pp. 306–312, 2010.
[20] M. S. Islam *et al.*, "Extracting structural features of rat sciatic nerve using polarization-sensitive spectral domain optical coherence tomography," *J. Biomed. Opt.*, vol. 17, no. 5, p. 056012, 2012.
[21] A. R. Duke, M. W. Jenkins, H. Lu, J. M. McManus, H. J. Chiel, and E. D. Jansen, "Transient and selective suppression of neural activity with infrared light," *Sci. Rep.*, vol. 3, p. 2600, Sep. 2013.
[22] L. A. Sermeus *et al.*, "Ultrasound-guided approach to nerves (direct vs. tangential) and the incidence of intraneural injection: A cadaveric study," *Anaesthesia*, vol. 72, no. 4, pp. 461–469, 2017.

DAEYOUNG CHOI received the B.E. degree in biotechnology from Yeungnam University, Gyeongsan, South Korea. He is currently a MD Researcher with the Electronics Engineering Department, Kyungpook National University, Daegu, South Korea. His research interests are in development of optical system for medical application, photoacoustic tomography, and development and applications for swept source optical coherence tomography.

JAEYUL LEE is currently pursuing the Ph.D. degree with the School of Electronics Engineering, Kyungpook National University, Daegu, South Korea. His research background includes optical imaging techniques, photoacoustic imaging techniques, photoacoustic microscopy, optical coherence tomography, and handheld instruments for optimization of the optical coherence tomography and photoacoustic microscopy systems.

MANSIK JEON received the Ph.D. degree in electronics engineering from Kyungpook National University, Daegu, South Korea, in 2011. He is currently an Assistant Professor with the School of Electronics Engineering, Kyungpook National University. His research interests are in the development of nonionizing and noninvasive novel biomedical imaging techniques, including photoacoustic tomography, photoacoustic microscopy, optical coherence tomography, ultrasonic imaging, handheld scanner, and their clinical applications.

JEEHYUN KIM received the Ph.D. degree in biomedical engineering from the University of Texas at Austin, USA, in 2004. He was a Post-Doctoral Researcher with the Beckman Laser Institute, University of California at Irvine. He is currently an Associate Professor with Kyungpook National University, Daegu, South Korea. His research interest is in biomedical imaging and sensing, neuroscience studies using multiphoton microscopy, photo-acoustic imaging, and other novel applications of sensors.